Surface azimuth estimation from solar irradiance on tilted surfaces

Inti Piccioli[1], Gonzalo Abal[1] and Mathieu David[2]

[1] Laboratorio de Energía Solar, Universidad de la República, Salto (Uruguay)

[2] PIMENT Laboratory, Universitè de La Rèunion, St. Denis, Reunion Islands (France)

Abstract

Azimuth misalignment of receiver surfaces is a frequent source of uncertainty when working with solar irradiance measurements on tilted surfaces (GTI). Two complementary methods to estimate the true azimuth of a tilted surface from GTI data are implemented and evaluated; the first method being a new one, and the second a variation of a previously existing one. Ground data from an arrangement of tilted pyranometers with different azimuths, along with global horizontal, direct normal and diffuse horizontal irradiance (GHI, DNI and DHI) data, are used to validate the methods. The results show good agreement with nominal azimuth values, with typical uncertainties of a few degrees that increase with the nominal azimuth. Both methods are complementary since they have different strengths and weaknesses.

Keywords: global solar irradiance, azimuth misalignment, tilted surfaces

1. Introduction

Non-concentrating tilted surfaces for solar energy collection maximize the received energy when oriented towards the equator (zero azimuth). Interpretation of measurements of solar irradiance on these tilted surfaces (GTI) relies on the accurate orientation of the surfaces. For several reasons, the actual surface azimuth (angle between the normal to the surface and the local meridian) may differ from its nominal value, and GTI data is misinterpreted. When measurements of global irradiance on the tilted surfaces are not available, radiation transposition models can be used to estimate GTI on arbitrary oriented surfaces from global horizontal irradiance (GHI). These models require knowledge of the surface orientation for optimal performance. Surface azimuth measurements are usually made with common GPS devices, with magnetic compasses or by using the shadow of a vertical rod at solar noon. In practice, these methods can be inaccurate by several degrees. Furthermore, GTI pyranometers mounted on remote measuring sites are exposed to extreme weather conditions which can result in azimuth misalignments of the tilted surface, which in a long time series might vary over time. These azimuth-related errors can have a direct impact on the energy output estimates and affect the economic analysis of solar energy systems.

Recently, this problem was addressed in Barbier et al., 2019 by proposing a method for estimating the misalignment of tilted surfaces by minimizing the error of a transposition model for estimating GTI at different azimuths. The estimates for GTI are derived from clear-sky estimates of GHI and its diffuse component (DHI) obtained from the McClear model

doi:10.18086/swc.2021.39.02 Available at http://proceedings.ises.org

(Lefèvre et al., 2013), available at the Copernicus Atmosphere Monitoring Service (CAMS). To the best of our knowledge, we have found no other work on this topic.

In this paper, a new method (referred as Method PA) is described which can estimate the azimuth using only GTI data, and provides an estimate for its uncertainty. For a long time series this method is also capable of detecting changes in azimuth over time. A second method (referred here as Method BBSD) is also implemented and evaluated; it is a variant of that proposed in Barbier et al., 2019, based on the ESRA clear-sky model (Rigollier et al., 2000) and using ground data instead of satellite estimates. Controlled-quality laboratory data from two sites with eight tilted surfaces of well-known tilt and azimuth angles are used to evaluate both methods.

2. Data

The main source of GTI data comes from an array of pyranometers mounted on a specially designed semi-hemispheric structure at the PIMENT Laboratory (Reunion Islands, France). This one-year dataset includes 1-min resolution GTI data for several tilt and azimuth angles and was originally used for the evaluation of transposition models (David et al., 2013). Aside from the GTI data, five months of simultaneous GHI, DHI and direct normal irradiance (DNI) data are also included. The location, period and angles for this dataset are listed in Table 1. Other details on this measurement campaign can be found in (David et al., 2013). Additionally, data from the Solar Energy Laboratory (LES http://les.edu.uy, last access: 20/09/2021) in Salto, Uruguay, comprising two series of measurements of GTI corresponding to two tilt angles and zero azimuth are considered. This dataset spans five years (2016-2020) of 1-minute resolution simultaneous GHI, DHI and DNI data. The location and other details for both sites are listed in Table 1.

Tab. 1: Location, labeling and orientation of the different datasets evaluated in this work. For the Southern Hemisphere, surface azimuth is zero for north-oriented surfaces, negative for surfaces facing North-East, and positive towards North-West.

Site	Lat (°)	Lon (°)	Alt (m)	Label	Period	(Tilt, Azimuth) (°)
Reunion Island	-21.33	-55.50	76	PIM	11/2008-12/2009	$(20,0);(20,-30);$ $(40,0);(40,\pm 30);(40,\pm 60)$
Salto, Uruguay	-31.28	-57.91	56	LES	01/2016-12/2020	$(30,0);(45,0)$

GTI, GHI and DHI data for both sites are mostly from class A (spectrally flat) Kipp & Zonen pyranometers. The exception is that at the LES site GTI was measured using CMP6 pyranometers (class B, spectrally flat), see Table 2. The GHI and DHI instruments were ventilated and DNI was measured with Kipp & Zonen CHP1 pyrheliometers mounted on SOLYS2 solar trackers at both sites. The trackers where equipped with a shading ball that blocks the beam irradiance on the DHI pyranometers. These instruments received maintenance on a daily basis.

Details on the labeling and orientation of the different surfaces considered are shown in Table 2, where the number of clear days selected for Method PA of azimuth detection are also included.

Tab. 2: Location, labeling and orientation of the different datasets evaluated in this work. For the Southern Hemisphere, surface azimuth is zero for north-oriented surfaces, negative for surfaces facing North-East, and positive towards North-West.

Label	Tilt and Azimuth	Sensor model	Site	Clear days selected (method PA)
G40_60E	(40°,-60°)	CMP11	PIMENT	20
G40_30E	(40°,-30°)	CMP11	PIMENT	35
G20_30E	(20°,-30°)	CMP11	PIMENT	33
G45_0	(45°,0°)	CMP6	LES	26
G40_0	(40°,0°)	CMP11	PIMENT	28
G30_0	(30°,0°)	CMP6	LES	35
G20_0	(20°,0°)	CMP11	PIMENT	24
G40_60W	(40°,60°)	CM11	PIMENT	21
G40_30W	(40°,30°)	CMP11	PIMENT	26

3. Methods for surface azimuth estimation

3.1. Method PA

For sun-facing tilted surfaces, GTI data under clear sky conditions as a function of the hour angle ω have well defined daily maximums. Let ω^* be the hour angle that maximizes GTI; if is zero, the surface is oriented towards the equator and its azimuth equals zero (if the proper azimuth convention for each hemisphere is used, a zero azimuth corresponds to a surface oriented towards the equator in both hemispheres). For an observer in the southern hemisphere, if ω^* is negative the surface is facing North-East and maximum GTI occurs before solar noon; if ω^* is positive the surface is facing North-West and maximum GTI occurs after solar noon, as shown in Fig. 1. Thus, ω^* has the relevant information about the true surface azimuth.

If simultaneous GHI data are available, automatic clear sky detection algorithms may be used to find days with clear intervals containing the GTI maximum ω^*. Otherwise, a careful visual inspection of the data is required to select the clear days for which the GTI maximum is well defined. Fig. 1 shows an example of clear sky GTI data for three surface orientations from the PIMENT dataset, together with GHI data.

A three-step procedure is followed to find the true azimuth: (i) first the suitable days from the GTI time series are selected, and an auxiliary function $\gamma = f(\omega^*)$ that relates the surface azimuth with the hour angle that maximizes GTI is determined for each of them. (ii) the hour angle ω^* for which GTI has a maximum is determined, together with its corresponding azimuth candidate $\gamma = f(\omega^*)$. Finally, (iii) the final surface azimuth γ is determined by averaging the azimuths candidates for all days and its uncertainty is also characterized using

the standard deviation.

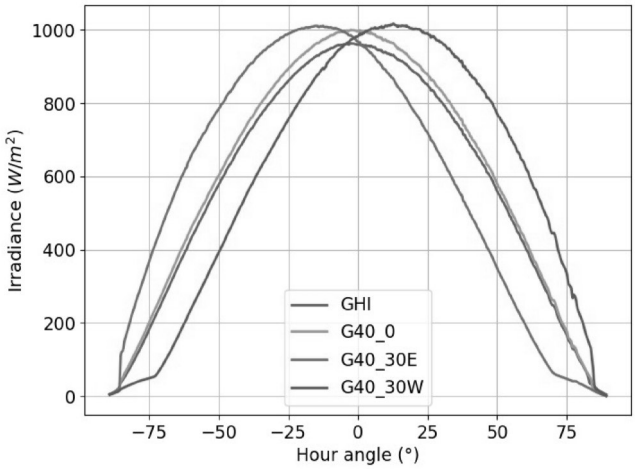

Fig. 1: GTI data for different surface orientations from the PIMENT dataset, corresponding to a clear day in March 2009.

3.1.1. Clear day selection and parametrization of the auxiliary function $\gamma = f(\omega^*)$

Starting with high resolution (1-minute or smaller intervals) GTI data, days with clear-sky conditions around the GTI maximum are selected. This step must be performed manually unless a set of reliable, simultaneous GHI data is available. In this case, automatic detection algorithms for clear sky conditions can be used. Otherwise, careful visual inspection of the GTI data is required.

For each selected clear day, the function $\gamma = f(\omega^*)$ that relates the hour angle that maximizes GTI with the surface azimuth, is parametrized. This function depends on the site and also (weakly) on the day number (n=1,2,... 365) and so it must be determined for each selected day in the GTI series.

The parametrization of this function relies on a clear sky model and proceeds as follows. For each selected day, horizontal clear-sky estimates for GHI, DHI and DNI are generated. We use the ESRA clear-sky model (Rigollier et al, 2000) for this task due to its simplicity and the fact that it requires only one parameter (the Linke turbidity, T_L). For a range of surface azimuths, which must include the "true" azimuth, the Perez transposition model (Perez et al, 1993) is applied to estimate the corresponding clear-sky GTI values. We favor this refined transposition model instead of other simpler models, for technical reasons which are clarified below. The ground is assumed to be a perfect diffuse isotropic reflector with a fixed surface reflectance of 0.25.

Locally adjusted daily T_L cycles for the Uruguayan region, calculated in (Laguarda and Abal, 2016), were used for the LES site. Linke turbidity data from the Reunion Island were obtained from the PVLIB Python library (Holmgren et al., 2018), which is based on generic global estimates (Remund et al. 2003).

As can be seen in Fig. 2 (left panel), the GTI estimates obtained using the ESRA clear-sky estimates and the simple isotropic transposition model (Liu and Jordan, 1961) show significant variations in the solar times of their maxima for different values of T_L. The right panel of Fig. 2, uses the same ESRA clear sky estimates but with the Perez transposition model, which results in a weaker dependence on T_L and is therefore more suitable for this

procedure than the simple isotropic model.

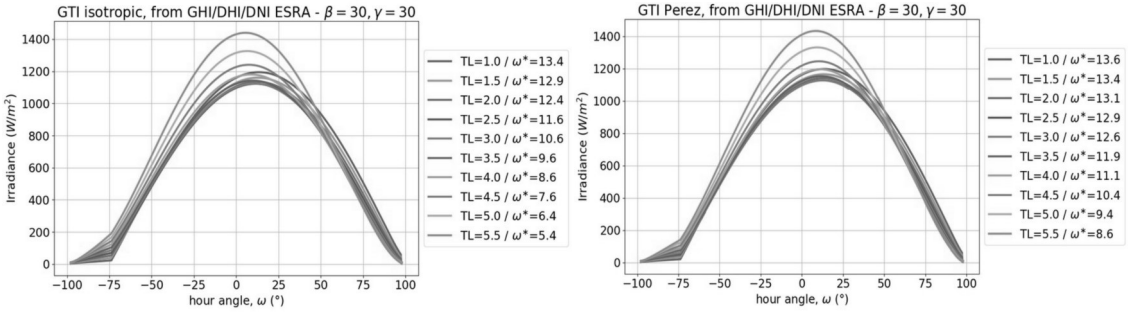

Fig. 2: Comparison between calculated GTI from GHI/DHI/DNI ESRA clear sky estimates with different Linke turbidity values, for a 30° tilt / 30° azimuth surface. Left: GTI from the isotropic transposition model. Right: GTI from the Perez model.

To parametrize the function $\gamma = f(\omega^*)$ we propose a fitting of the form $\gamma = a \times \tan(b\omega^*)$, where the angles γ and ω^* are in radians. The coefficients (a, b) are obtained using least squares optimization and, as mentioned before, have a weak seasonal dependence on the day of the year. If the nominal value of the surface azimuth is known, the fitting can be improved by performing it in a small neighbourhood of this nominal value.

Two examples of this procedure are shown in Fig. 3, for +30° and -60° azimuth angles. An indicator of the goodness of fit, coefficient R^2 defined as $R^2 = 1-(SSres/SStot)$ where SSres is the sum of squares of the residuals and SStot is the total sum of squares, was calculated for each day selected. It ranged from 0.9995 to 0.9997, which ensures that the fitting is accurate. It can be seen that the absolute slope of the function increases with the absolute surface azimuth, which means that small variations in ω^* imply large variations in the estimated azimuth (hence amplifying the uncertainty of the method for large angles). This slope is almost vertical for azimuths close to 90°, which makes this method unsuitable for extreme deviations from γ=0. This is not a strong limitation, since energy absorbing surfaces are usually oriented towards the equator.

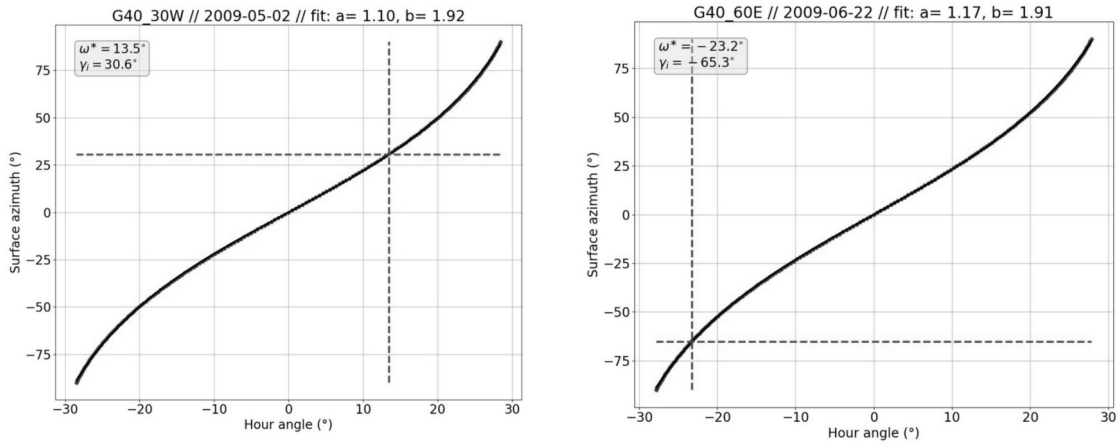

Fig. 3: Two examples of the fitting and evaluation of the $f(\omega^*)$ function, for different orientations. Coefficients of the proposed fitting are given for those particular days, as well as the R^2 coefficient. Results show good agreement with the surface azimuth nominal values. The range of azimuths used for the fitting is between -90° and +90°.

3.1.2 Estimation of ω^*

Once the suitable days with clear-sky conditions around the GTI maxima have been selected and the parameters *(a, b)* have been determined, the hour angle ω^* for which the maximum is attained must be found. For each of these days, a suitable interval centered around the solar time when GTI is maximum is selected. As can be seen from Fig. 4, at the 1-minute timescale, raw data can have small ripples or noise which may affect the determination of the solar time for the maxima. In order to smooth out these irregularities, a quadratic polynomial of the form $\gamma = a_2\omega^2 + a_1\omega + a_0$ is fitted to the data in this interval. Outliers are rejected by an iterative procedure in which data points that differ from the fitting curve by more than a certain tolerance value are labeled as outliers and discarded. New polynomial is fitted to the remaining data and the procedure is repeated until all the data satisfies the criteria. In actual practice, it converges after a few iterations. Finally, the hour angle that maximizes the fitting curve, $\omega = -a_1/2a_2$, is the best estimate for ω^* on the given day.

3.1.3 Estimation of the surface azimuth over time

By substitution of ω^* into the corresponding function $\gamma=a\times\tan(b.\omega^*)$, the azimuth estimate γ_i for clear day i is obtained. Fig. 3 shows two examples of such substitution. Repeating this process for each clear day in the GTI series with clear skies at maximum GTI, a series of azimuth estimates results. If no drastic changes of azimuth are identified over time, the simple average of this series is the final estimate of the surface azimuth, γ, and the standard deviation provides an estimate of the accuracy u of the method.

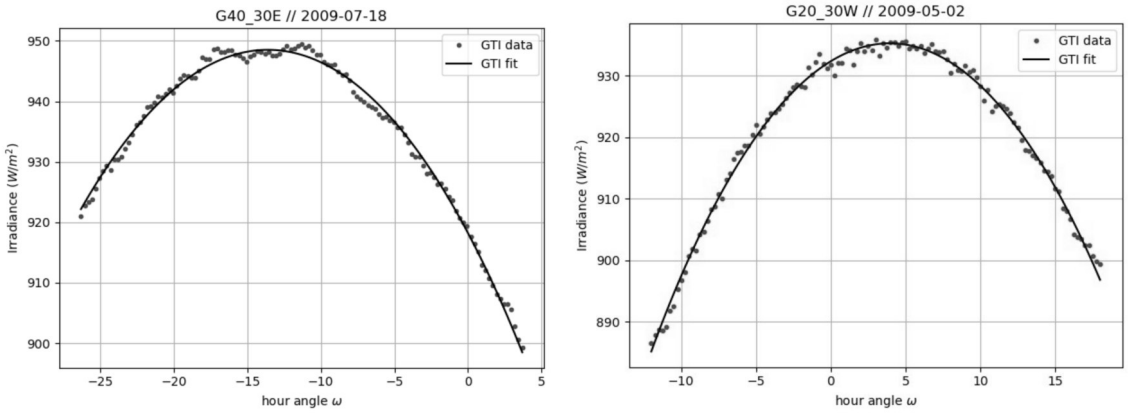

Fig. 4: Examples of GTI 1-minute data as a function of the hour angle (in degrees) near their maxima, for two different orientations. Left: 40° tilt and -30° azimuth; right: 20° tilt and 30° azimuth. Data are fitted in order to obtain ω^*, which will be used to estimate the azimuth.

3.2. Method BBSD

As mentioned, this method was first proposed in (Barbier et al., 2019) using both surface orientation angles, and satellite-based clear sky estimates for the horizontal irradiance components. It is based on the comparison between measured and estimated GTI from a suitable transposition model. Ideally, it requires simultaneous GHI, DHI and DNI data at 1-hour or subhour time scales. The clear-sky estimated and measured GTI values are compared for several azimuth values around the nominal or expected azimuth, and the azimuth that minimizes the deviations is selected.

For this paper, this procedure has been implemented using a 1-minute dataset with simultaneous (GHI, DHI, DNI, GTI) measurements and it can be described in four steps, as follows:

(i) The data was filtered according to the quality control criteria proposed in (Perez-Astudillo et al, 2018), which include the relevant Baseline Solar Radiation Network (BSRN) tests. In particular, data corresponding to solar altitudes less than 10° were rejected in order to reduce the impact of cosine errors. Other reasonable quality control filtering procedures can be followed for this initial stage.

(ii) An automated clear-sky detection algorithm (Reno and Hansen, 2016) was used to identify clear sky data by comparison of measured GHI and the clear-sky estimates from the ESRA model. Clear sky filtered data thus selected were averaged into 10-minute intervals, since this method does not require high time-resolution data. An averaged interval is computed only if 2/3 of the data that comprise it passed the filters and the clear sky detection; otherwise it is labeled as NaN.

(iii) GTI is estimated from GHI, DHI and DNI data for a range of surface azimuths, which must include the nominal value. We refer to these estimates as $GTI_e(\gamma)$. The anisotropic Perez transposition model is used for this purpose, since it is one of the best transposition models and better describes the anisotropic characteristics of the cloudless sky (D. Yang, 2016).

(iv) The modeled $GTI_e(\gamma)$ are compared with the measured GTI using the Relative Root Mean Square Deviation (rRMSD), expressed in relative terms (%) with respect to the mean of the measurements $\overline{GTI}$:

$$\mathrm{rRMSD} = \frac{100}{\overline{GTI}} \times \sqrt{\frac{1}{N}\sum_{i=1}^{N}(GTI_{e,i} - GTI_{m,i})^2} \qquad \text{(eq. 1)}$$

where N is the number of samples, $GTI_{e,i}$ are the estimated values and $GTI_{m,i}$ are the measured GTI values. The azimuth that minimizes the rRMSD is our first estimate of the true surface azimuth.

A standard random sampling and cross validation procedure is performed (one thousand iterations with 50/50 split of the data set for training and evaluation subsets) and the average azimuth γ is the best estimate from this method. Its standard deviation is a measure of the statistical uncertainty (variability within the ensemble) associated with this method and it is usually negligible compared with the total uncertainty.

Conceptually, this method is simpler than the method PA described in Section 3.1, which has the advantage of requiring only GTI measurements for the site. However, under PA, the measurements must have high time resolution (1-minute intervals) and must include several clear sky periods with well defined GTI maximums.

3.2.1. Data filtering

For this method, good quality ancillary data (GHI and DHI or DNI) must be available in order to avoid selecting clear samples which contain traces of clouds, since this can affect the accuracy of the azimuth determination.

For the PIM experiment, 78669 simultaneous diurnal 1-minute samples of the three components (GHI, DHI, DNI) and GTI for several orientations were jointly available for a period of six months between February and July of 2009. For the LES site, 1434844 diurnal 1-minute records are available for a five year (2016-2020) containing the three components (GHI, DHI, DNI) and GTI for two tilt angles and zero azimuth (see Tables 1 and 2).

The same set of filters (F1 to F18 proposed in Pérez-Astudillo et al. 2018) are applied independently to the (GHI, DHI, DNI) components in both datasets. These filters include the relevant BSRN filters (Long and Shi, 2006) and are complemented with filters to detect other conditions, such as misalignment of the tracker. Modified parameters are used as needed. The last filter, F19, is a visual inspection mask which removes a few (less than 0.1% of the samples) data artifacts and astronomical events (such as eclipses) from the datasets.

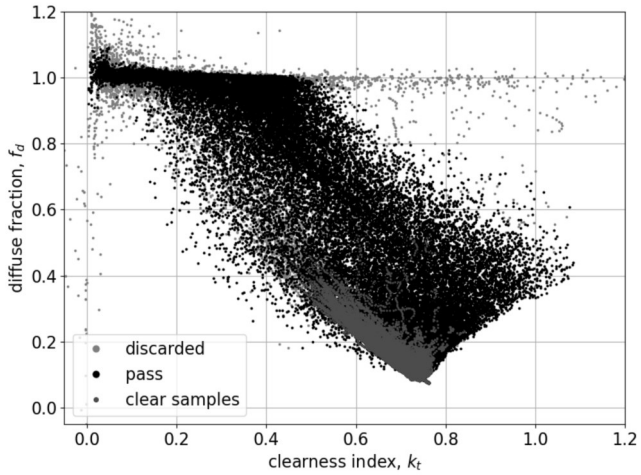

Fig. 5: Diffuse fraction vs clearness index diagram for the PIM site. Data discarded by the filtering process is greyed out and the selected clear samples are highlighted in red.

After the filtering process and clear-sky data selection, 26142 clear samples were selected for the PIM site (all orientations). For the LES data, after integration to 10-min intervals, 12910 clear-sky records for tilt β=30° and 20623 records for tilt β=45° were selected. Fig. 5 shows the diffuse fraction, f_d = *DHI/GHI* versus the clearness index k_t (GHI normalized by the horizontal extraterrestrial irradiance), with the discarded data greyed out and the selected clear-sky samples highlighted in red for the PIM experiment. Fig. 6 shows how the clear-sky detection algorithm operates on a GHI series.

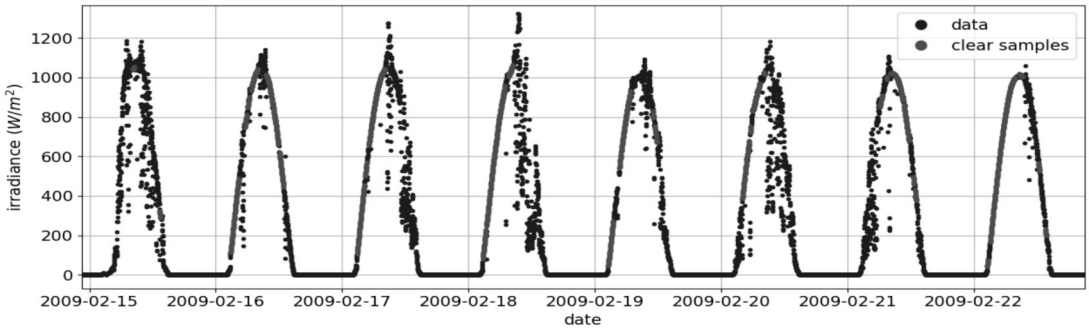

Fig. 6: 1-min GHI time series, with the clear samples highlighted in red, for the PIM site.

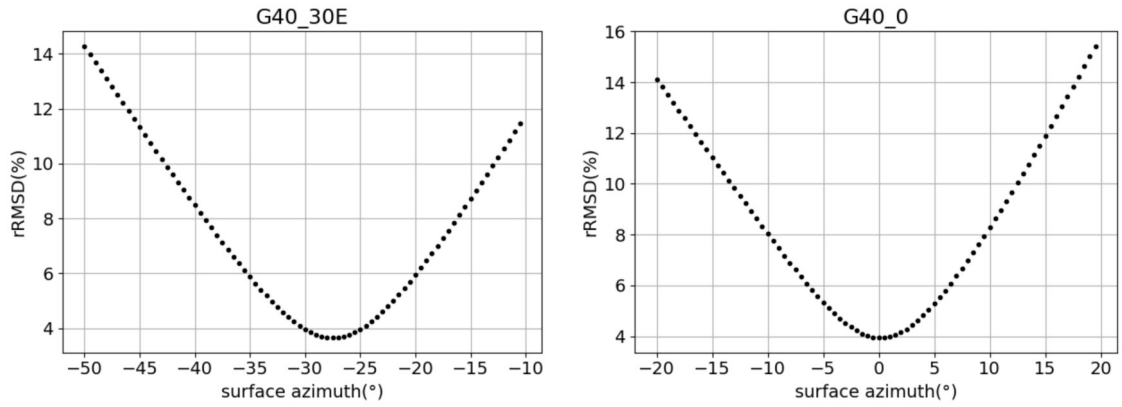

Fig. 7: rRMSD obtained by comparison of measured GTI and the Perez model's estimate, as a function of the surface azimuth, for two tilted planes with different nominal azimuths. Data from the PIMENT experiment.

3.2.2 Examples of the optimization procedure

Two examples of the optimization procedure which leads to the best surface azimuth are shown in Fig. 7, both showing that the rRMSD has a well defined minimum and the target azimuth is accurately determined. In (Barbier et al. 2019) this method was applied in the context of a large PV array in a two dimensional space (tilt, azimuth) using Mc Clear (Lefèvre et al., 2013) estimates for clear-sky information available at CAMS. In our case, ground measurements for GHI, DHI and DNI are used and the tilt angle is fixed. In contrast to method PA, this method is unable to identify changes in azimuth over time and thus should be applied only in cases in which the azimuth is fixed.

4. Results

Azimuth estimates from Method PA for all the orientations from the PIMENT experiment are shown in Figure 8, throughout the time span for this data. The azimuth estimates, standard deviations and the deviation from true value are shown in Table 3 for both datasets.

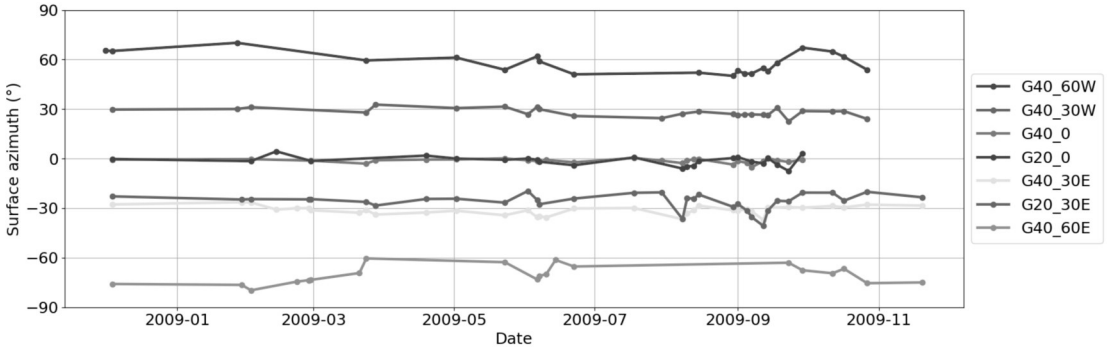

Fig. 8: Azimuth estimates for the PIMENT data using method 1. Labels are to be interpreted from Table 2.

Tab. 3 Estimated azimuths ɣ for all orientations, together with their respective uncertainty u, given by the standard deviation of all the estimated azimuths for method PA, and by the standard deviation σ from the cross-validation procedure for method BBSD. Also included, the difference *d* between the estimated azimuth and the nominal value. The last row shows the absolute average of u and of the deviations.

		Method (PA)			Method (BBSD)		
Label	**Dataset**	**ɣ(°)**	**u(°)**	**d(°)**	**ɣ (°)**	**u(°)**	**d(°)**
G40_60E	PIM	-70.2	5.6	10.2	-60.4	0.2	0.4
G40_30E	PIM	-31.2	2.7	1.2	-27.6	0.2	-2.4
G20_30E	PIM	-25.8	4.8	-4.2	-20.6	0.3	-9.4
G45_0	LES	-1.3	1.8	1.3	-0.9	0.2	0.9
G40_0	PIM	-1.3	1.2	1.3	0.0	0.1	0.0
G30_0	LES	-1.5	1.5	1.5	-2.0	0.2	2.0
G20_0	PIM	-1.3	2.8	1.3	1.8	0.2	1.8
G40_60W	PIM	58.0	6.1	-2.0	49.0	0.1	-11.0
G40_30W	PIM	28.1	2.5	-1.9	27.5	0.0	-2.5
average		-	3.2	2.8	-	0.2	3.4

As can be seen from Figure 8, if surface azimuth variations occur over time, method PA can detect those changes while method BBSD can be used on sub-intervals with well defined azimuth, provided GHI and diffuse fraction data is available.

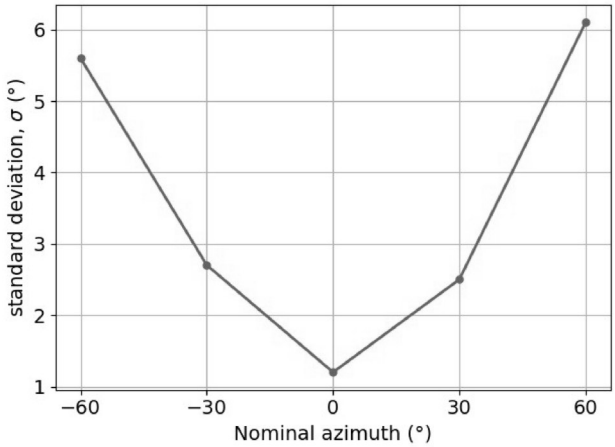

Fig. 9: Standard deviation from method 1 as a function of the nominal azimuth of the surface, for the 40° tilt surfaces (PIMENT).

The standard deviation of method PA (shown as *u* in Table 3) describes the variability of the estimated azimuth over time. If the nominal azimuth is known to be fixed over this time period, this observed variability can be used as the true uncertainty for the method. Its average value of 3.2° is similar to the average absolute deviation of the method. This uncertainty increases with the surface azimuth (see Fig. 9 for the 40° tilt experiments). Since only a few tilt angles have been considered, there is no clear evidence of a similar

dependence on the uncertainty with surface tilt.

The statistical standard deviation of method BBSD (shown as u in Table 3) is an order of magnitude smaller than the observed deviations and therefore is not useful as an uncertainty estimate. Finally, the absolute deviations from method PA are smaller in most cases than those from our implementation of method BBSD.

5. Conclusions

Two methods for the estimation of surface azimuths were implemented and validated against data from tilted surfaces with nominal azimuth values between 60º East and 60º West. The first method (labelled PA) is new and it allows to estimate the surface azimuth using only 1-minute resolution GTI data and clear sky estimates from a reliable model. The method also provides the estimated uncertainty, if the azimuth is known to be fixed for the duration of the GTI measurements. If changes in azimuth take place, the method can detect these changes over time. This makes it a useful method to perform quality checks on remote measuring stations which can be affected by severe weather conditions. The accuracy of this method is similar or better than our implementation of a second method (labelled BBSD), based on horizontal measurements of GHI and its diffuse fraction.

The PA method cannot be used to detect azimuth orientations of surfaces that are not facing the sun (i.e. azimuths greater than 90°), since it relies on the existence of a maximum on the GTI curve for clear days. For small misalignments, the usual scenario in several applications, this method performs well, with an average uncertainty of 3.2º over several tested orientations. Its uncertainty increases with the nominal azimuth of the surface, and for the -60° surface azimuth (east-oriented), the departure of the estimate from the nominal value (d) is larger than the uncertainty u.

The BBSD method (also evaluated here) is unable to detect changes of azimuth over time, but it is less complicated in terms of calculations. It requires ground data for GTI, GHI, DHI (or DNI), or clear-sky satellite estimates. The time resolution of the data is not a critical issue.

Both methods of azimuth estimation are complementary, in the sense that they differ in strengths and weaknesses. Work is underway in order to refine the first method and address the cases where there's conflicting outputs between the two methods, especially for large azimuths.

6. References

Barbier, T., Blanc, P., Saint-Drenan, Y., 2019. Software correction of angular misalignments of tilted reference solar cells using clear-sky satellite open data. EU PVSEC 2019, Marseille, France. hal-02291410.

David, M., Lauret, P., Boland, J., 2013. Evaluating tilted plane models for solar radiation using comprehensive testing procedures, at a southern hemisphere location. Renewable Energy 51, 124-131.

Holmgren, W., C. Hansen and M. Mikofski (2018). PVLIB Python: A Python package for modeling solar energy systems. Journal of Open Source Software 3 (29): 884.

Laguarda, A., Abal, G., 2016. Índice de Turbidez de Linke a partir de irradiación solar global en Uruguay. Avances en Energías Renovables y Medio Ambiente, Vol. 20, pp 11.35-11.46, 2016.

Lefèvre, M., Oumbe, A., Blanc, P., Espinar, B., Qu, Z., Wald, L., Homscheidt, M. S. and Arola, A. (2013). McClear: a new model estimating downwelling solar radiation at ground level in clear-sky conditions. Atmospheric Measurement Techniques, European Geosciences Union, 6 , 2403–2418. doi:10.5194/amt-6-2403-2013.

Liu, B., Jordan, R., 1961. Daily insolation on surfaces tilted towards the equator. ASHRAE Trans. 67, 526–541.

Long C.N. and Shi Y. 2006. The QCRad Value Added Product: Surface Radiation Measurement Quality Control Testing, Including Climatologically Configurable Limits. Atmospheric Radiation Measurement Program, Technical Report, ARM TR-074. Available at http://www.arm.gov/publications/tech_reports/doe-sc-arm-tr-074.pdf

Perez-Astudillo, D., Bachour, D., Martin-Pomares, L., 2018. Improved quality control protocols on solar radiation measurements. Solar Energy 169, 425-433.

Perez, R., Seals, R., Michalsky, J., 1993. All-weather model for sky luminance distribution-Preliminary configuration and validation. Sol. Energy 50 (3), 235-245.

Remund, J., Wald, L., Lefèvre, M.,, Ranchin, T., Page, J., 2003. Worldwide Linke turbidity information. ISES Solar World Congress 2003, Jun 2003, Göteborg, Sweden. 13 p. hal-0046579.

Reno, M., Hansen, C., 2016. Identification of periods of clear sky irradiance in time series of GHI measurements. Renewable Energy, 90, p. 520-531

Rigollier, C., Bauer, O, Wald, L., 2000. On the clear sky model of the ESRA - European Solar Radiation Atlas with respect to the Heliosat method. Solar Energy, 68 (1), pp.33-48. hal-00361373.

Yang, D, 2016. Solar radiation on inclined surfaces: Corrections and benchmarks. Solar Energy 136, pp. 288-302. https://doi.org/10.1016/j.solener.2016.06.062